Adaptive modeling of environmental effects in modal parameters for damage detection in civil structures

Hoon Sohn[a], Mark Dzwonczyk[b], Erik G. Straser[a], Kincho H. Law[a], Teresa Meng[b] and Anne S. Kiremidjian[a]

[a]Department of Civil and Environmental Engineering
Stanford University, Stanford, CA 94305, U.S.A.

[b]Department of Electrical Engineering
Stanford University, Stanford, CA 94305, U.S.A.

ABSTRACT

Many researchers have proposed damage detection techniques that exploit changes in modal parameters to identify the extent and location of damage in large structures. These analyses, however, generally neglect the effects of environmental changes on modal parameters. Such environmental effects include changes in loads, boundary conditions, temperature, and humidity. Data from real bridge structures indicate that the effects of environmental changes can be significant. In fact, these changes can often mask more subtle structural changes caused by damage. This paper examines a linear adaptive model that may discriminate the changes of modal parameters due to temperature changes from those caused by structural damage or other environmental effects. Data from the Alamosa Canyon Bridge in the state of New Mexico were used to demonstrate the effectiveness of the adaptive filter for this problem. Results indicate that a linear four-input (two time and two spatial dimensions) filter of temperature can reproduce the natural variability of the frequencies with respect to time of day. Using this simple model, we attempt to establish a confidence interval of the fundamental frequency for a new temperature profile in order to discriminate the natural variation due to temperature.

Keywords: Adaptive filter, modal parameters, temperature effect, Alamosa Canyon Bridge, damage detection

1. INTRODUCTION

Many techniques have been proposed to identify the extent and location of damage in large structures using changes in the structures' modal parameters. These methods typically determine the baseline parameters through acquisition of forced or ambient vibration test data. Damage detection is then based on the premise that damage in the structure will cause changes in the measured vibration data. Existing methods, however, neglect the important effects of environmental changes on the underlying structure. Changes in load, boundary conditions, temperature and humidity can have a significant effect on the underlying natural frequencies of large civil structures. In fact, the changes in the modal parameters due to environmental factors can be far larger than those caused by structural damage. During damp weather, for example, concrete bridges in the United Kingdom are reported to absorb considerable moisture; The moisture increases their mass altering their natural frequencies.[1] Before damage detection systems can be reliably employed to monitor real structures, the non-stationarity of the modal parameters must be quantified.

This paper mainly studies the thermal effects on the non-stationary responses of bridges. Very few researchers have addressed these problems. Churchward and Sokal[2] attempted to predict the temperature distribution within bridge sections and to determine longitudinal expansion and vertical deflection based on a three-year monitoring of a poststressed concrete section of a bridge. The measured environmental parameters include ambient air temperature, solar radiation, hours of sunshine and the temperature on the top surface of the section. It is found that the temperature profile can be reasonably represented through only two design variables, namely maximum differential temperature and base temperature. Wood[1] reported that the bridge responses were closely related to the structural temperature based on the vibration tests of five bridges in the United Kingdom. Analyses based on data compilation of bridge tests suggested that the variability of the asphalt elastic moduli due to temperature effects was a major contributor to the changes in the structural stiffness.

Correspondence to Hoon Sohn, Department of Civil and Environmental Engineering, Stanford University, Stanford, CA 94305-4020, USA. E-mail: sohnhoon@leland.stanford.edu

Turner[3] tested a three-span foot-bridge which consisted of one central 16m and two 8m spans with 2m by 0.8m reinforced T section concrete decks. To determine any correlation between temperature and changes in vibrational response, three transverse modes of the central span and two transverse modes of one side span were monitored over a thirty-month period at approximately four-month intervals. The natural frequencies of this small bridge appeared unaffected by temperature changes. Moorty[4] attempted to relate the response of bridges exposed to thermal environmental conditions. An analytical model was developed to obtain the temperature-induced movements and the associated stress in bridges. A field test was conducted on the Sutton Creek Bridge in Montana, and the movements obtained both from the analytical model and the measured values showed significant extensions of the bridge deck as temperature increased.

This paper presents an adaptive filter that accommodates the changes in temperature to the damage detection system of a large-scale bridge. This system determines modal frequencies using conventional modal analyses, but is able to adapt its prediction of the underlying natural frequencies of the structure based upon a time-temperature profile. This may allow the system to discriminate the changes of modal parameters due to temperature changes from those caused by other environmental factors or structural damage. For example, when the measured frequencies move outside the predicted confidence intervals, the system can provide a reliable indication that structural changes are likely caused by factors other than thermal effect. Actual data were collected from the Alamosa Canyon Bridge in the New Mexico and used to train and test the system.

2. DESCRIPTION OF THE ALAMOSA CANYON BRIDGE TEST

The Alamosa Canyon Bridge is located near the town of Truth or Consequences in southern New Mexico and is approximately aligned in the north and south direction. This bridge has seven independent spans and each span consists of a concreted deck supported by six W30x116 steel girders. The top flanges of the girders are embedded in the concrete slab. The roadway in a span is approximately 7.3 m (24 ft) wide and 15.2 m (50 ft) long. Along the length of each span, four sets of crossing braces are equally spaced. Figure 1 depicts a side view of the Alamosa Canyon Bridge. More detailed description of the bridge can be found in Farrar *et al.*.[5]

A new bridge has been constructed adjacent to this *old* Alamosa Canyon Bridge and since that time the tested bridge has not been used for regular traffic. During the past three years, however, the bridge has been tested several times. An attempt to characterize the natural variability of modal parameters was conducted in 1996.[5] The inherent uncertainty in the measured modal parameters was also studied using experimental test data from the bridge.[6]

This current study uses the results of vibration tests conducted on July 27-August 2, 1996 and July 21-25, 1997, referred to as the *first* and *second* data sets, respectively. The first data set was used to train the adaptive filter while the second data set was used to test the predictor. For both tests, only one span was implemented with sensors and tested. A total of 31 accelerometers were placed on the concrete deck and on the girders below the bridge. Five accelerometers were spaced along the length of each girder. Since there were six girders, a total of 30 accelerometers were placed on the girders. The last accelerometer was placed near the driving point. The time histories of accelerations and an excitation force were recorded, and the frequency response functions (FRFs) were computed from the time histories. The FRFs were calculated for the range of 0 to 50 Hz with the resolution of 0.0625 Hz. Thirty averages were used for most FRFs. An impact hammer which weighted approximately 53.4 N (12 lbs) was used to excite the bridge. The data acquisition for each test usually took 30-45 minutes. The modal parameters were extracted employing eigensystem realization algorithm (ERA).[7] Approximately nine meaningful modes were identified from ERA within the range of 0-30 Hz.

At the same time, temperature measurements were made on nine different locations across the center of the span. Figure 2 illustrates a cross-section view of the bridge and the distribution of the thermometers, as follows: The Bottom West Outdoor (BWO) sensor was attached to the outside of the west-end exterior girder at the mid height of the wed. The Bottom West Indoor (BWI) sensor was located on the inside bottom flange of the west-end exterior girder. The Bottom Center (BC) sensor was taped the beneath of the concrete deck at the center of the span. The Top West Outdoor (TWO) sensor was located next to the concrete curb at the west-end of the deck. The Top West Indoor sensor (TWI) was placed on the top of the west-end guard rail. The four remaining sensors were placed on the east end of the span symmetrically to the west-end sensors. All sensors were protected from the direct contact with sunshine either by the bridge itself or by shades made from duct tape and cups.

The first vibration test was performed every two hours over a 24-hour time period to investigate the change of modal parameters with respect to time of a day. The air was dry throughout the test. Farrar *et al.*[5] showed that the

first measured frequency varied approximately 5% during the 24-hour test period, and the change in the measured first frequency was correlated to the temperature difference across the deck. Similar variations and correlation with deck temperature difference were observed for the other modes of the bridge. Table 1 summarizes the measured first frequencies and temperatures from the first vibration test. The test started on July 31 1996 at 09:15 and ended on August 1 at 9:22. The temperature of a given time in Table 1 is an average of the thermometer readings before and after each vibration test. In addition to the temperature effect, traffic, winds, deterioration of the bridge and other environmental conditions could produce changes of the modal parameters. However, since the bridge has not been used during the test period, it is assumed that any changes of the modal parameters are the result of the temperature changes.

The second testing was conducted about one year after the first testing. Vibration tests were performed eleven times every two hours from four in the morning to midnight. A note is in order about the weather conditions prior to the second vibration test; it had been raining hard from approximately 10:00 PM the previous night of the testing until 3:00 AM. When the data acquisition was started at 4:00 AM, rain was sufficient to produce ponds of water near the curbs and drainage paths were blocked by debris. The concrete deck was sufficiently cracked such that a fair amount of moisture might have been absorbed by the bridge. When the second vibration test was conducted, no significant stiffness deterioration were observed since the first testing. In the second testing, no temperature sensor was placed at the bottom center. The other thermometers were placed almost in the same locations as those of the first testing. Table 2 summarizes the results from the second vibration test. The second test started on July 22 at 04:00 and ended at midnight.

3. MODEL FORMULATION

The first challenge in the analysis was to determine an appropriate signal processing architecture for predicting the (unknown) variation in modal frequencies as a function of temperatures. Prediction of the first natural frequency was selected as a target for this study and it was presumed that the temperature changes of the bridge were mainly responsible for the variation of that frequency. This assumption seems reasonable since the bridge was no longer in service and there was no significant change of weather conditions on the first test day (that is, there was no traffic, significant wind or ground excitations, etc.). Observations of the bridge data coupled with some engineering judgment led to three additional assumptions that appear simplistic but are important factors in the design of the signal processing architecture: (1) changes in the modal parameters are *linearly* proportional to changes in temperature; (2) the mass of the bridge forced the change in modal parameters to lag the temperature, that is, the bridge took some time to *warm up* and *cool off*; and (3) the geographical (north-south) orientation of the structure with respect to the sun suggests that the temperature of the west end of the bridge will lag the temperature of the east end.

Given these assumptions, a linear predictor appears to be a simple, but potentially very effective, system architecture. A linear filter simply creates a linear one-to-one mapping on input and output pairs. It affords explicit calculation of the filter coefficients using a simple matrix calculation and allows future modification of these coefficients using adaptive least-mean squares error minimization. The filter operates in two modes: *training* and *prediction*. Training is described in Section 3.1. Section 4 validates the applicability of the filter for prediction by testing its performance on the second data set.

3.1. Training the Linear Filter Model

This section discusses the method of *Least Mean Squares* (LMS) error minimization that is used to estimate the coefficients of the linear filer. The architecture of the linear filter takes a subset of the temporal and spatial temperature profiles as inputs and delivers a single output that represents the estimated, or predicted, fundamental frequency (the smallest natural frequency of the bridge). Determining the appropriate subset of the available temperature profiles is termed the *variable selection problem* and is discussed in Section 3.2. Since the bridge is oriented in the north and south direction, one would expect the modal parameters of the structure to differ depending upon the average structure temperature and the distribution of that temperature across the span. Furthermore, the instantaneous outside air temperature may not be important in the predictor design, but clearly a longer-term average will be important. Therefore, the rate of change in temperature should be taken into account.

The filter models the relationship between the selected bridge temperature inputs, $\mathbf{x} = [x_1\ x_2\ \ldots\ x_r]^T$, a column vector of r inputs, and its measured fundamental frequency, y_d, at that temperature profile as linear:

$$y_d = w_0 + \mathbf{x}^T \mathbf{w} + \epsilon \tag{1}$$

where w_0 is bias or offset, $\mathbf{w}$ is a column vector of coefficients that weights each temperature input, and ϵ is the *filter error*. Suppose that n observations are available and let $\mathbf{x}(i)$ and $y_d(i)$ denote the ith input-output pairs. We now have a matrix development of Equation (1) to present n observations in matrix notation:

$$\mathbf{y}_d = \mathbf{X}\mathbf{w} + \boldsymbol{\epsilon} \tag{2}$$

where

$$\mathbf{y}_d = \begin{bmatrix} y_d(1) \\ y_d(2) \\ \vdots \\ y_d(n) \end{bmatrix}, \ \mathbf{X} = \begin{bmatrix} \mathbf{x}^T(1) \\ \mathbf{x}^T(2) \\ \vdots \\ \mathbf{x}^T(n) \end{bmatrix} = \begin{bmatrix} 1 & x_1(1) & x_2(1) & \dots & x_p(1) \\ 1 & x_1(2) & x_2(2) & \dots & x_p(2) \\ \vdots & \vdots & \vdots & & \vdots \\ 1 & x_1(n) & x_2(n) & \dots & x_p(n) \end{bmatrix}, \ \boldsymbol{\epsilon} = \begin{bmatrix} \epsilon(1) \\ \epsilon(2) \\ \vdots \\ \epsilon(n) \end{bmatrix}$$

LMS error minimization is employed to estimate the filter coefficients. We wish to find the vector of the filter coefficients $\hat{\mathbf{w}}$ that minimizes the expected value of the energy of the filter error.[8]

$$\begin{aligned} &\min_{\mathbf{w}} \ E\left[\, \epsilon(i)^2 \,\right] \\ &\rightsquigarrow \hat{\mathbf{w}} = \mathbf{R}^{-1}\mathbf{p} \end{aligned} \tag{3}$$

where $\mathbf{R}(= E[\mathbf{x}\mathbf{x}^T])$ is the *autocorrelation* of the random input vector $\mathbf{x}$, and $\mathbf{p}$ $(= E[y_d\mathbf{x}^T])$ is the *cross-correlation* between the desired output and the input vector. Equation (3) is called the *Wiener-Hopf equation* and used to determine the *estimated* coefficients, $\hat{\mathbf{w}}$, for a given set of input-output pairs.

One should note that the actual filter output error that results after applying the Wiener-Hopf equation depends upon the number of input-output mappings (n) that are used to determine $\hat{\mathbf{w}}$ and the dimension of $\hat{\mathbf{w}}$, p. If the filter is underspecified, that is, the number of input-output pairs is less than the dimension of $\hat{\mathbf{w}}$, then the Wiener-Hopf equation will produce an unlimited number of different $\hat{\mathbf{w}}$'s that result in zero error ($\boldsymbol{\epsilon} = \mathbf{0}$). This means that there exists an infinite number of weights that will produce zero error for the given observation sets.

Since the training data set was fixed for this study, we decided to reduce the dimension p. In the derivation of Equation (1), all input variables are assumed to be influential in predicting the output response. However, in most practical applications, the analyst must check the significance of each input and determine some optimal subset of inputs from a pool of *candidate* inputs. This variable selection is equivalent to pruning irrelevant or redundant inputs from the filter of Figure 3, and the procedure is addressed in the following subsection.

3.2. Input Variable Selection

In order to consider both the time and spatial variations of temperature, we decide to define the temperature readings at the current time T_i, and at one step previous time T_i' as an initial pool of candidate input variables. Let k denote the size of this input pool. While the number of candidate input variables is eighteen (nine temperature readings at the current time and the other nine from the one step previous time), the number of observations from the first vibration test is thirteen ($n = 13$). Therefore, the selection of input variables should be conducted to reduce the size of the filter before any estimation of the filter coefficients. In general, a model with smaller number of input variables is more desirable because the variable of the prediction $\hat{y}$ increases as the number of inputs increases. Furthermore, addition of extra inputs increases the costs of data collection and model maintenance.

First, the correlation of the nine sensor readings and the measured fundamental frequency is investigated. Table 3 presents the resulting correlation matrix. The correlation matrix shows that temperatures at the top east indoor (T_3)

and at the top west indoor (T_4) are very closely related (Table 1 shows the relation between T_i's and thermometer locations). The temperature at the bottom west indoor (T_6) is also strongly correlated to the temperature at the bottom west outdoor (T_8). T_4 is deleted from the filter model because T_3 has a larger correlation with the observation output y_d than T_4. For the same reason, T_6 is kept in the model and T_8 is excluded. Since the second data set did not measure the temperature at the bottom center, the variable search did not include T_9. Now, the number of candidate input variables becomes twelve (k=12).

Next, an exhaustive search of all possible subsets of the remaining input variables is conducted. If the intercept weight w_o is always included, a total of 2^k models should be examined. In this example, there are 2^{12} (=4096) possible models. This study employs adjusted R^2 statistic for evaluating subset models. To explain adjusted R^2 statistic, let R_p^2 denote the coefficient of multiple determination for a subset model with p weightings. Computationally

$$R_p^2 = \frac{SS_R(p)}{S_{yy}} = 1 - \frac{SS_E(p)}{S_{yy}} \tag{4}$$

and

$$S_{yy} = \sum_{i=1}^{n}(y_i - \bar{y})^2, \quad SS_R(p) = \sum_{i=1}^{n}(\hat{y}_i - \bar{y})^2, \quad SS_E(p) = \sum_{i=1}^{n}(y_i - \hat{y})^2 \tag{5}$$

where S_{yy}, $SS_R(p)$ and $SS_E(p)$ denote the *total sum of squares*, the *regression sum of squares*, and the *residual sum of squares* of p size of subset model, respectively. Furthermore, $\bar{y}$ denotes the mean of the output observation ($\bar{y} = \sum_{i=1}^{n} y_d(i)/n$). R_p^2 increases as additional input variables are introduced to the model and reaches the maximum when $p = k + 1$.

The analyst might use this criterion by adding input variables to the model up to the point where an additional variable is not useful in that it provides only a small increase in R_p^2. However, since R_p^2 increases as p increases, using R_p^2 is straightforward to determine the optimal model. To avoid this difficulty, this study prefers to use an adjusted R^2 statistic defined as

$$\bar{R}_p^2 = 1 - \left(\frac{n-1}{n-p}\right)(1 - R_p^2) \tag{6}$$

Note that $\bar{R}_p^2$ statistic does not necessarily increase as p increases. Consequently, one can consider the model that has the maximum $\bar{R}_p^2$ value an optimum subset model.

Table 4 shows the three best models that maximize $\bar{R}_p^2$ for each given number of inputs, $3 \leq r \leq 9$. The first column of Table 4 shows the identification numbers of the examined subset models. The best models for each given r ($3 \leq r \leq 9$) are retained for further comparison (models 1, 4, 7, 10, 13, 16 and 19). Note that three models with five input variables (models 13, 14 and 15) and the best model with four inputs (model 16) have larger R_p^2 values than the best models for $r = 7$ and $r = 6$ (models 7 and 10). Therefore models 14 and 15 are also retained for further investigation. The filter system appears to approach the optimal architecture when the size of inputs is around four or five ($4 \leq r \leq 5$).

The F statistic test is conducted for the remaining models (models 1, 4, 7, 10, 13, 14, 15, 16 and 19). The F statistic test determines if there is a linear relationship between the output and any of the input variables. $F_0 > F_{\alpha,r,n-r-1}$ implies that at least one of the inputs contributes significantly to the model. Here, F_0 is a ratio of the regression mean square (MS_R) to the residual mean square (MS_E). Furthermore, the regression mean square (MS_R) and the residual mean square (MS_E) are SS_R/r and $SS_E/(n-r-1)$, respectively. $F_{\alpha,r,n-r-1}$ is found from a statistical table of the F distribution. A detailed description for the F statistic test can be found in Reference 9. The results of the F statistic test shows that all the selected models have significant linear relationship between the inputs and output. However, the passing of the F statistic test does not necessarily indicate that the model examined is an appropriate one for predicting the output. Further tests of model adequacy are required.

The t statistic examines the significance of the individual filter coefficient to the model given that the model retains the other inputs. The hypotheses for testing the significance of any input, such as w_i, are

$$\begin{aligned} H_0 &: w_i = 0 \\ H_1 &: w_i \neq 0 \end{aligned} \tag{7}$$

If $|t_0| > t_{\alpha/2,n-r-1}$, the hypothesis H_0 is rejected implying that the examined input contributes significantly to the model. Here, $t_0 = \hat{w}_i / \sqrt{\hat{C}_i \, \sigma^2}$, C_i is the ith diagonal element of $(X^T X)^{-1}$, and $\hat{\sigma}^2$ is an unbiased estimate of the sum of squared errors of the system.

$$\hat{\sigma}^2 = \sum_{i=1}^{n} \frac{(y_d(i) - \hat{y}(i))^2}{n-p} \tag{8}$$

The value of $t_{\alpha,r,n-r-1}$ is found from a statistical table of the t-student distribution. Note that this examines only the marginal contribution of one input given the other inputs are in the model. The results of the t statistic test shows that only for models 4, 16 and 19, the hypothesis $H_0 : \beta_j = 0$ is not rejected. This indicates that the other models contain redundant inputs that can be deleted from the models.

Finally, model 16 with inputs T_3, T_7, T_2' and T_3' is selected as a *satisfactory* model for the prediction of the second data set since (1) the $\bar{R}_p^2$ value of model 16 is comparable to that of model 4 or better than model 19, (2) this model passes both F and t statistic tests, and (3) model 16 has only half as many inputs as model 4. From Equation (3), the LMS estimator of $\hat{\mathbf{w}}$ is computed for model 16:

$$\hat{\mathbf{w}} = [\hat{w}_o \; \hat{w}_{T_3} \; \hat{w}_{T_6} \; \hat{w}_{T_2'} \; \hat{w}_{T_3'}]^T = [7.509 \quad 0.007694 \quad -0.001992 \quad -0.01575 \quad 0.01044]^T \tag{9}$$

The selection of model 16 and the estimated filter coefficients in Equation (9) reveals that (1) the response change of the Alamosa Canyon Bridge lags the temperature of the bridge (the temperatures of two hours before the current time contribute more significantly to the change of the current frequency than the temperatures at the current time: $\hat{w}_{T_2'}$ and $\hat{w}_{T_3'}$ are approximately ten times larger than $\hat{w}_{T_3}$ $\hat{w}_{T_7}$), and (2) the temperature gradient between the top west outdoor and the top east indoor ($0.01044T_3'$-$0.01575T_2'$) largely influences the variable of the fundamental frequency. This supports the observation in Reference 5 that the changes in modal frequencies are related to the temperature differentials across the deck.

Figure 5 shows how well the selected model 16 reproduces the fundamental frequency from the first data set which is employed for the training of the filter. Note that only three temperature readings at TWO, TWI and BEO out of nine total thermometers are necessary to reasonably estimate the change of the fundamental frequency. One might apply the input selection scheme presented here to address the placement problem of measurement: how many and where should the measurement sensors be placed to obtain better prediction of the desired output response?

4. PREDICTION USING A TRAINED MODEL

The adaptive filter established in the previous section was used to predict the fundamental natural frequency of the bridge. The predicted value is then used to discriminate the changes of the fundamental natural frequency caused by temperature effects from changes caused by other environmental effects or potential damage of the structure. For example, let $\mathbf{x}_0$ denote a vector of new temperature readings. A point prediction $\hat{y}_0$ of the fundamental natural frequency at the temperature becomes

$$\hat{y}_0 = \mathbf{x}_0^T \hat{\mathbf{w}} \tag{10}$$

where $\hat{\mathbf{w}}$ is the weight vector determined in Equation (9).

One cannot expect a perfect match of the prediction and the measured modal parameters because of incompleteness of the model, insufficient training data sets, uncertainties in actual testing and measurements and so on. Of broader importance, however, one can compute a confidence interval around the point prediction $\hat{y}_0$ to account for the inherent uncertainties. A 100(1-α)% confidence interval for the predicted output at the given input observation, namely $\hat{y}_0$ in this case, is a classic regression analysis problem. In Reference 9, the confidence interval is computed as

$$\hat{y}_0 - t_{\alpha/2,n-p}\sqrt{\hat{\sigma}^2(1 + \mathbf{x_0^T(X^TX)^{-1}x_0})} \le y_0 \le \hat{y}_0 + t_{\alpha/2,n-p}\sqrt{\hat{\sigma}^2(1 + \mathbf{x_0^T(X^TX)^{-1}x_0})} \tag{11}$$

Once the filter is trained, the newly collected frequency can be compared against the point prediction value and the confidence interval. If the fundamental natural frequency falls outside a 100(1-α)% confidence interval, then

one may suspect with 100(1-α)% confidence that some changes in underlying structural characteristic are caused by damage or other environmental effects. In Table 5, the predicted value of the fundamental natural frequency and a 95% confidence interval were computed for the different time of temperature profiles from the second data set. The first column of the table shows the starting time of each testing, and the second and third columns present the lower and upper bounds of the confidence interval, respectively. These bounds are computed from Equation (11). $\hat{y}$ and y_d in Table 5 denote the predicted frequency from Equation (10) and the measured frequency from the second testing, respectively.

In predicting new observations, one should be careful not to extrapolate beyond the input variable region containing the training data set. A model that fits well inside the the region of the original data may perform poorly outside that region. In a multi-dimensional input space, it is difficult to decide if an input variable point lies inside or outside the region of the original data. The diagonal elements of the *hat* matrix $\mathbf{H}(= \mathbf{X}(\mathbf{X}^T\mathbf{X})^{-1}\mathbf{X}^T)$ are employed to detect a hidden extrapolation point.[9] Let the largest diagonal value of the hat matrix $\mathbf{H}$ to be h_{max}, and define the smallest convex containing all of the training data points as the input variable hull (IVH). The relative distance of any input variable vector $\mathbf{x}_0$ to the centroid of the IVH is reflected by

$$h_0 = \mathbf{x}_0^T(\mathbf{X}^T\mathbf{X})^{-1}\mathbf{x}_0 \tag{12}$$

If $h_0 > h_{max}$, the point is outside the IVH and requires an extrapolation. The value of h_0 depends both on the Euclidean distance of the corresponding point from the centroid of the training data and on the density of points in the IVH. In the last column of Table 5, the h_0 value of each input is compared to h_{max}. Only the last five points corresponding to time 16:00, 18:00, 20:05, 21:54 and 24:00 are interpolation points. We presume that only these data points inside the IVH are reliable for the prediction.

The measured natural frequencies from the second data sets, and the upper and lower bounds of the 95% confidence interval are plotted in Figure 5. From Figure 5, one can observe that the measured frequencies corresponding to the interpolation points are consistently lower than the associated lower bounds of the 95% prediction interval (except the one at time 16:00). This implies that the stiffness of the structure deteriorated or the mass of the structure increased. Considering the fact that the Alamosa Canyon Bridge is a concrete bridge, it had visible cracks over the deck, and there was a severe rain from 10 PM the night before to the second testing until 3 AM of testing, it is very possible that these consistent decreases of the fundamental natural frequency were caused by the increase of the bridge mass as the Alamosa Canyon Bridge absorbed significant amounts of moisture. Assuming that the change of the bridge mass is solely responsible for the decrease of the fundamental frequency, the increase of mass is approximately estimated as 1.62%. Several bridge tests in the United Kingdom report that a concrete bridge can absorb considerable amounts of moisture during damp weather, which can consequently increase the mass of the bridge.[1]

5. SUMMARY AND DISCUSSION

This paper has presented an adaptive filter for predicting changes in modal parameters of a full-scale bridge due to environmental temperature. Data from the Alamosa Canyon Bridge in New Mexico were employed to demonstrate the applicability of the adaptive filter. The vibration tests were conducted during the summer in 1996 and summer in 1997. The first data set from the 1996 test was used to train the adaptive filter while the second data set from the 1997 test was used to test prediction performance.

Changes in the fundamental frequency are found linearly correlated with temperature readings from different parts of the bridge. The filter uses spatial and temporal temperature distributions to determine changes in the fundamental frequency. The simplicity of the filter belies its importance: the filer is able to account for the non-stationarity in structure modes caused by an environmental factor. A linear filter with two spatially-separated temperature measurements and two temporally-separated temperature measurements reproduces the variation of the fundamental frequency of the first data set.

From the trained filter system, a prediction interval of the fundamental frequency for a new temperature profile is developed and applied to the second data set. The system defines a confidence interval of future values of modal parameters in order to discriminate between variations caused by temperature changes and those indicative of structural change or other environmental effects. The comparison of the prediction intervals obtained from the first data set and the measured frequencies from the second test data reveals that the bridge experienced a statistically

significant decrease in the fundamental frequency. Considering the fact that there was a severe rain from 10 PM the previous night of the second testing until 3 AM of the testing, it is very possible that this consistent decrease of the frequency was caused by the increase of the bridge mass as the Alamosa Canyon Bridge absorbed significant amount of moisture.

It should be kept in mind that the filter system presented was developed for a particular bridge under particular environmental conditions. Further testing is required to fully validate the linear model. Although this study has been limited to a single external variable (temperature), the approach might be extendible to other environmental effects. To control for other environmental conditions and account for larger-scale seasonal variations, tests should be conducted during different times of the year as well as different times of a day, and measurements for other environmental factors should be obtained. Furthermore, a continuous data collection system would allow the filter coefficients to be more reliably updated, and to shrink the size of the confidence intervals. Reliable damage detections must account for the significant non-stationary environmental processes.

ACKNOWLEDGMENTS

The authors wish to express their sincere thanks to Dr. Charles R. Farrar and Dr. Scott W. Doebling of the Los Alamos National Laboratory for providing the experimental data of the Alamosa Canyon Bridge. This research was sponsored by the National Science Foundations under Grant No. CMS-95261-2 and the National Aeronautics and Space Administration under Grant No. NAG2-1065.

REFERENCES

1. M. G. Wood, *Damage Analysis of Bridge Structures Using Vibrational Techniques.* PhD thesis, Department of Mechanical and Electrical Engineering, The University of Aston in Birmingham, UK, 1992.
2. A. Churchward and Y. J. Sokal, "Prediction of temperatures in concrete bridges," *ASCE, Journal of Structural Division* **107**, pp. 2163–2176, 1981.
3. J. D. Turner, *An Experimental and Theoretical Study of Dynamic Methods of Bridge Conditioning Monitoring.* PhD thesis, University of Reading, UK, 1984.
4. S. Moort and C. W. Roeder, "Tempeature-dependent bridge movements," *Journal of Structural Engineering* **118**, pp. 1090–1105, 1992.
5. C. R. Farrar, S. W. Doebling, P. J. Cornwell, and E. G. Straser, "Variability of modal parameters measured on the Alamosa Canyon bridge," in *The Proceeding of the 15th International Modal Analysis Conference*, pp. 257–263, (Orlando, FL), 1997.
6. S. W. Doebling, C. R. Farrat, and R. S. Goodman, "Effects of measurement statistics on the detection of damage in the Alamosa Canyon bridge," in *The Proceeding of the 15th International Modal Analysis Conference*, pp. 918–929, (Orlando, FL), 1997.
7. J. N. Juang, "An eigensystem realization algorithm for modal parameter identification and model reduction," *Journal of Guidance, Control, and Dynamics* **8**, pp. 620–627, 1985.
8. B. Widrow and S. D. Stearns, *Adaptive Signal Processing*, Prentice-Hall, Englewood Cliffs, New Jersey, 1985.
9. D. C. Montgomery and E. A. Peck, *Introduction to Linear Regression Analysis*, John Wiley and Sons Inc., 1991.

Figure 1. A Side View of The Alamosa Canyon Bridge

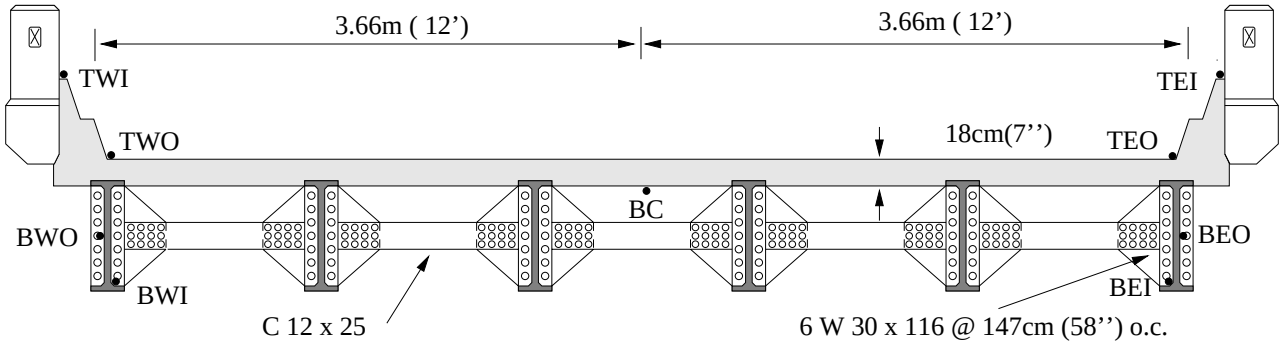

Figure 2. A Cross Section View and Thermometer Locations of The Alamosa Canyon Bridge

Table 1. Summary of The First Data Set

Time	1st Freq.	Temperature (F^o)								
	(Hz)	TEO (T_1)	TWO (T_2)	TEI (T_3)	TWI (T_4)	BEI (T_5)	BWI (T_6)	BEO (T_7)	BWO (T_8)	BC (T_9)
09:15	7.556	76.00	90.70	93.30	95.90	83.55	77.20	103.7	75.55	77.45
11:30	7.621	85.80	106.15	101.10	99.70	93.90	84.50	93.90	83.30	83.10
13:12	7.475	108.15	115.60	100.65	103.00	93.55	91.20	93.20	91.85	88.60
15:13	7.343	109.60	110.70	102.00	102.60	92.80	93.70	93.60	95.50	94.60
17:52	7.394	104.35	99.25	97.40	99.25	91.20	95.05	92.60	96.05	98.35
20:09	7.376	88.00	87.00	74.40	76.05	77.80	78.90	79.50	79.50	91.35
21:20	7.334	85.90	86.40	76.10	77.55	79.95	80.35	80.00	79.45	89.95
23:29	7.356	79.60	81.50	72.70	74.20	75.00	75.60	75.30	74.30	80.50
01:21	7.328	79.55	79.35	70.05	72.05	75.20	75.10	74.85	74.75	80.70
03:19	7.353	74.55	75.15	65.85	66.65	70.25	71.70	72.15	70.85	77.20
05:19	7.381	72.85	72.85	64.15	65.50	68.80	70.00	70.15	68.90	74.10
07:03	7.389	70.85	73.85	66.90	68.10	66.70	67.85	73.80	67.35	72.10
09:22	7.577	74.45	92.75	94.00	93.20	83.90	77.55	102.00	75.50	76.00

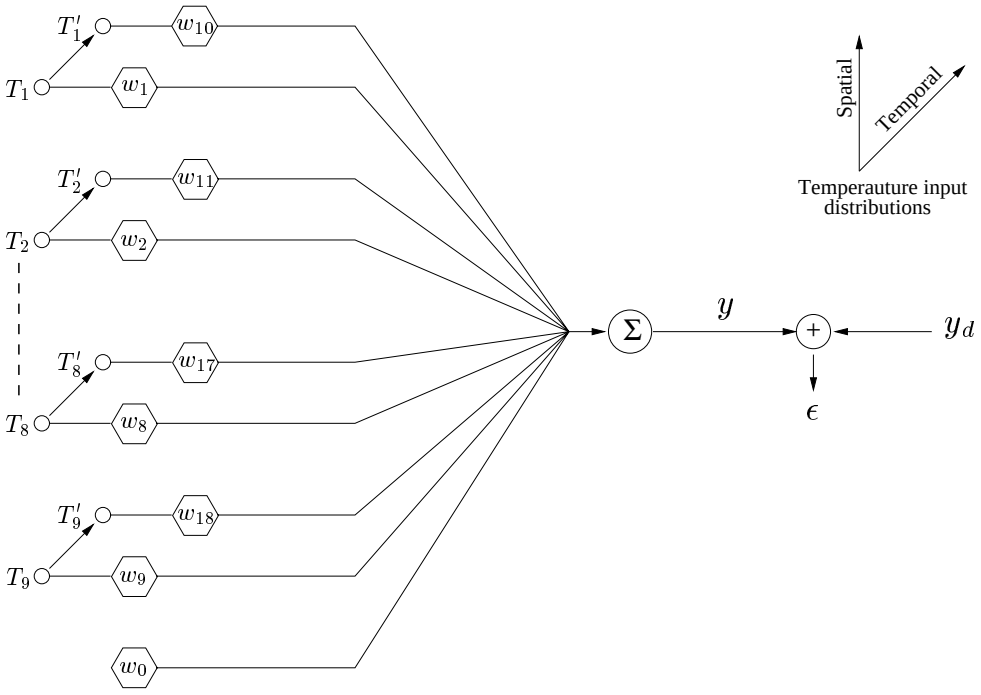

Figure 3. A Linear Adaptive Filter

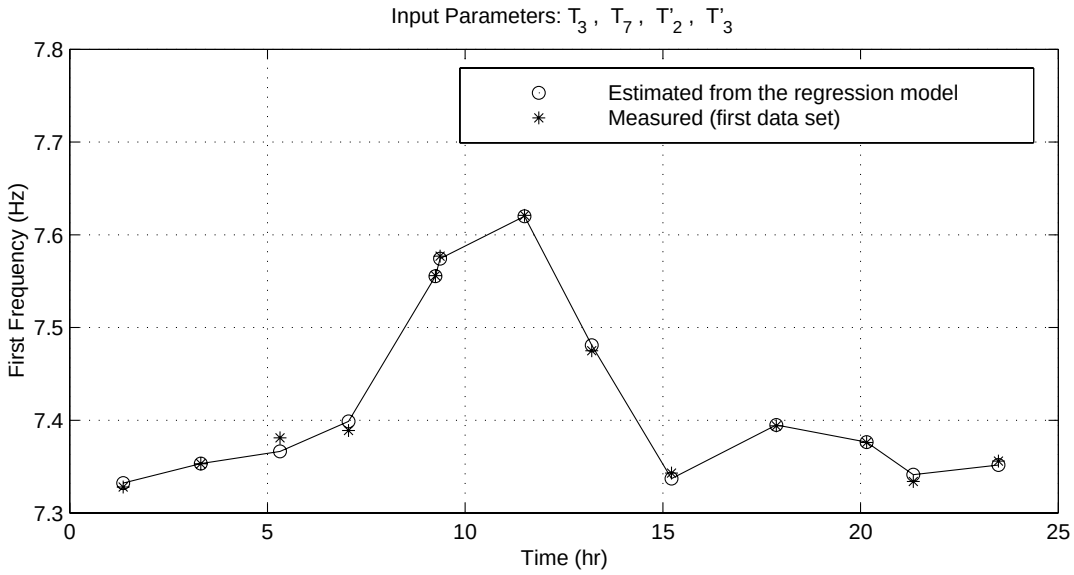

Figure 4. Reproduction of The Fundamental Frequency Using A Linear Filter

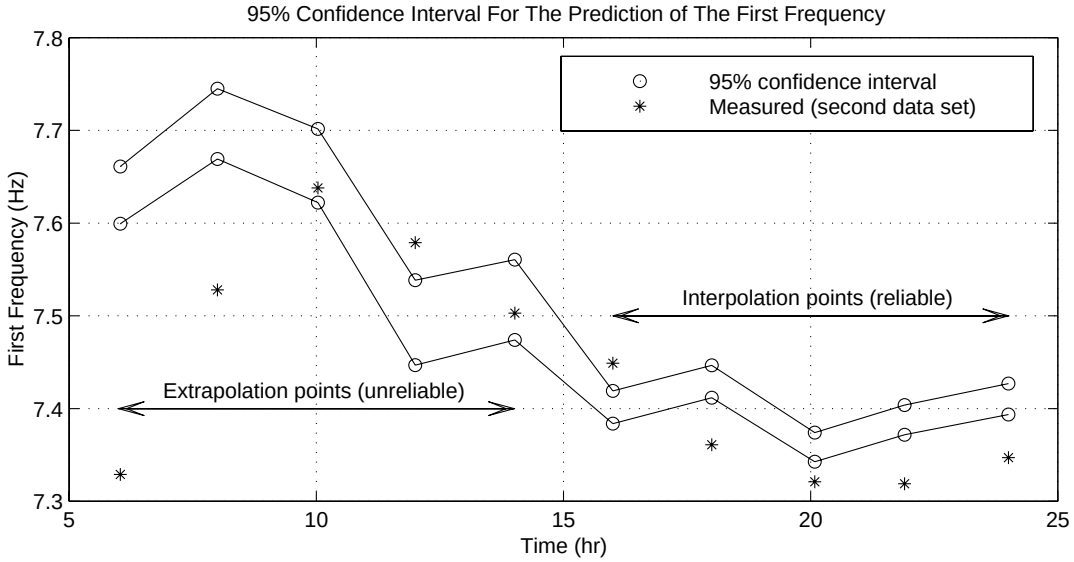

Figure 5. Prediction of The Fundamental Frequency Using A Linear Filter

Table 2. Summary of The Second Data Set

Time	1st Freq.	Temperature (F^o)								
	(Hz)	TEO (T_1)	TWO (T_2)	TEI (T_3)	TWI (T_4)	BEI (T_5)	BWI (T_6)	BEO (T_7)	BWO (T_8)	BC (T_9)
04:00	7.303	79.70	76.95	80.35	76.10	70.60	70.45	69.30	69.15	NA.
06:02	7.329	79.05	76.55	81.95	80.15	68.85	69.35	68.20	67.55	NA.
08:00	7.528	79.50	87.80	88.95	94.20	74.70	71.50	68.20	71.30	NA.
10:02	7.638	79.80	111.75	96.60	109.30	67.60	77.35	68.20	77.00	NA.
12:00	7.579	100.05	121.0	113.25	109.85	67.60	82.75	68.20	83.90	NA.
14:01	7.503	113.80	120.0	112.80	100.85	67.60	88.70	68.20	91.05	NA.
16:00	7.449	104.35	102.65	102.05	97.05	88.45	91.65	90.40	91.10	NA.
18:00	7.361	92.50	90.50	82.60	81.70	82.00	82.20	82.20	84.60	NA.
20:05	7.321	80.20	81.40	72.75	73.50	74.35	73.50	73.85	73.60	NA.
21:54	7.319	78.10	77.75	71.05	71.05	72.85	73.60	72.85	71.60	NA.
24:00	7.347	75.30	74.95	68.30	66.90	70.65	71.30	70.90	69.15	NA.

Table 3. Correlation of The Measured Natural Frequency and The Thermometer Readings

	y_d	T_1	T_2	T_3	T_4	T_5	T_6	T_7	T_8	T_9
y_d	1.000									
T_1	−0.097	1.000								
T_2	0.435	0.835	1.000							
T_3	0.608	0.684	0.941	1.000						
T_4	0.580	0.707	0.943	0.997	1.000					
T_5	0.485	0.787	0.969	0.966	0.966	1.000				
T_6	0.130	0.949	0.901	0.839	0.853	0.916	1.000			
T_7	0.741	0.396	0.750	0.910	0.909	0.807	0.605	1.000		
T_8	0.065	0.968	0.883	0.804	0.820	0.886	0.996	0.556	1.000	
T_9	−0.232	0.886	0.641	0.518	0.540	0.668	0.870	0.283	0.889	1.000

Table 4. The Best Three Models For Each Given Number Of Input Variables

#	r	$\bar{R}^2$	R^2_{pred}	Selected Input Variables											
1*	9	0.99801	0.96958	T_1	T_2		T_5	T_6		T'_1		T'_3	T'_5	T'_6	T'_7
2		0.99718	0.98144	T_1	T_2	T_3		T_6		T'_1		T'_3	T'_5	T'_6	T'_7
3		0.99678	0.98716	T_1	T_2			T_6		T'_1	T'_2	T'_3	T'_5	T'_6	T'_7
4*	8	0.99747	0.99374	T_1	T_2			T_6		T'_1		T'_3	T'_5	T'_6	T'_7
5		0.99517	0.98352	T_1	T_2	T_3		T_6		T'_1		T'_3	T'_5		T'_7
6		0.99324	0.97479		T_2	T_3			T_7	T'_1	T'_2	T'_3	T'_5	T'_6	
7*	7	0.99373	0.98514			T_3			T_7	T'_1	T'_2	T'_3	T'_5	T'_6	
8		0.99302	0.98485		T_2	T_3				T'_1	T'_2	T'_3	T'_5	T'_6	
9		0.99293	0.96718	T_1		T_3			T_7	T'_1	T'_2	T'_3	T'_5		
10*	6	0.99387	0.98804	T_1		T_3			T_7		T'_2	T'_3	T'_5		
11		0.99373	0.98639			T_3			T_7	T'_1	T'_2	T'_3	T'_5		
12		0.99369	0.98766			T_3		T_6	T_7		T'_2	T'_3	T'_5		
13*	5	0.99428	0.99112			T_3			T_7		T'_2	T'_3	T'_5		
14*		0.99414	0.99062	T_1		T_3			T_7		T'_2	T'_3			
15*		0.99386	0.99054		T_2	T_3			T_7		T'_2	T'_3			
16*	4	0.99410	0.99165			T_3			T_7		T'_2	T'_3			
17		0.98934	0.98275			T_3				T'_1	T'_2	T'_3			
18		0.98885	0.98131			T_3					T'_2	T'_3		T'_6	
19*	3	0.98809	0.97809			T_3					T'_2	T'_3			
20		0.94915	0.90774							T'_1		T'_3	T'_5		
21		0.94346	0.89520				T_5				T'_2	T'_3			

* Theses models are remained for further comparison and investigation.

Table 5. Comparison of the measured second data set and the predicted 95% confidence intervals

Time	95% Confidence		y_d	$\hat{y}$	Relative*	Check Extrapolation
	Lower	Upper			Error(%)	h (h_{max})
06:02	7.592	7.669	7.630	7.329	3.95	3.6004 (> 0.7686)
08:00	7.660	7.755	7.707	7.528	2.32	5.9233 (> 0.7686)
10:02	7.612	7.712	7.662	7.638	0.31	6.6219 (> 0.7686)
12:00	7.435	7.550	7.493	7.579	1.15	9.0997 (> 0.7686)
14:01	7.463	7.570	7.517	7.503	0.19	8.0356 (> 0.7686)
16:00	7.379	7.424	7.401	7.449	0.64	0.5026 (< 0.7686)
18:00	7.407	7.451	7.429	7.361	0.92	0.4734 (< 0.7686)
20:05	7.338	7.378	7.358	7.321	0.51	0.1836 (< 0.7686)
21:54	7.367	7.408	7.388	7.319	0.93	0.2384 (< 0.7686)
24:00	7.389	7.431	7.410	7.347	0.85	0.3396 (< 0.7686)

* Relative Error (%)=$100 \times |y - \hat{y}|/\hat{y}$